

VIP Very Important Paper

Special Issue



Bifunctional Oxygen Electrocatalysts for Lithium–Oxygen Batteries

Youngjoon Bae^{+, [a, b]} Hyeokjun Park^{+, [a, b]} Youngmin Ko^{+, [a, b]} Hyunah Kim^{+, [a, b]}
Sung Kwan Park,^[a] and Kisuk Kang^{*[a, b]}

Lithium–oxygen batteries have attracted great attention over the last few decades owing to their extraordinarily high theoretical energy density, which can potentially exceed that of current state-of-art lithium-ion batteries. However, lithium–oxygen batteries exhibit poor cycle stability, relatively low power capability and significantly large polarizations for both, the oxygen reduction reaction (ORR, discharge) and the oxygen evolution reaction (OER, charge). To address these issues, various catalysts for aqueous and non-aqueous lithium–oxygen batteries have thus been introduced, and some recent developments of bifunctional catalysts could simultaneously facilitate the ORR and OER, leading to great advance-

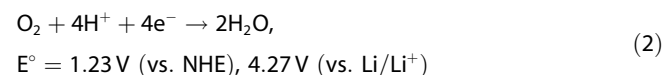
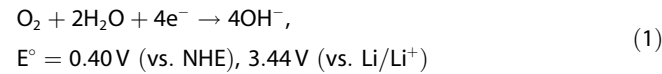
ments in the overall battery performance. Herein, we present a brief overview of recent progress in the development of bifunctional catalysts for lithium–oxygen batteries based on the current understanding of their working mechanism. Perovskite-type, spinel-type, and non-oxide catalysts and their use in aqueous lithium–oxygen batteries are reviewed. Recently reported bifunctional catalysts in non-aqueous lithium–oxygen batteries are also introduced, and the different roles of solid- and soluble-type catalysts are further discussed. Finally, we conclude by deliberating the design prospects and perspectives for efficient bifunctional catalysts for future lithium–oxygen batteries.

1. Introduction

With the ever-increasing global demand for energy sources and depletion of the current main energy supply of fossil fuels, vigorous efforts have been focused on the development of next-generation renewable and sustainable energy sources such as solar and wind energy for the production of electric energy.^[1–3] However, to enable the efficient use of these electric energy sources without being affected by obstructing factors such as time and weather, electrical energy storage systems are critical. Furthermore, the expanding markets for portable electronics and electric vehicles encourage the development of high-energy-density energy storage systems.^[4,5] Although Li-ion batteries currently dominate the energy storage market, the current state of their specific energy is regarded insufficient for future devices.^[6] Therefore, tremendous efforts have been devoted to developing energy storage systems with higher energy densities that can ultimately overcome the limits of Li-ion batteries.^[7–10] Among various candidates, lithium–oxygen ($\text{Li}–\text{O}_2$) batteries based on the Li/O_2 electrochemistry have been

spotlighted because of the theoretical specific energies of over 3500 Wh kg⁻¹, which result from the use of light elements instead of heavy transition metals and their relatively high theoretical voltage of approximately 3 V.^[11]

$\text{Li}–\text{O}_2$ batteries can be roughly categorized into two types depending on the electrolyte system: aqueous $\text{Li}–\text{O}_2$ batteries and non-aqueous $\text{Li}–\text{O}_2$ batteries. Aqueous $\text{Li}–\text{O}_2$ batteries are composed of Li metal, an aqueous electrolyte, an air electrode, and a separating layer between the Li metal and aqueous electrolyte to protect the Li metal from the side reactions with water in the aqueous electrolyte. Li^+ conducting solid electrolytes such as $\text{Li}_{1+x+y}\text{Al}_x\text{Ti}_{2-x}\text{Si}_y\text{P}_{3-y}\text{O}_{12}$ (LATP) have been used as the separating layer. Because LATP decomposes when in direct contact with Li metal, a conventional organic carbonate electrolyte is typically used as a buffer between the Li metal and LATP in most cases.^[12] Therefore, organic and aqueous electrolytes are often incorporated together as “hybrid” $\text{Li}–\text{O}_2$ batteries.^[11,12] While most of aqueous $\text{Li}–\text{O}_2$ batteries reported thus far are based on alkaline electrolyte, the major electrochemical reaction in the cathode can be altered depending on the pH of the electrolyte in aqueous $\text{Li}–\text{O}_2$ batteries. In basic electrolyte, H_2O and O_2 are reduced to form OH^- [Reaction (1)], whereas in acidic electrolyte, H^+ and O_2 are reduced to produce H_2O [Reaction (2)] during the discharge reaction, i.e., oxygen reduction reaction (ORR).

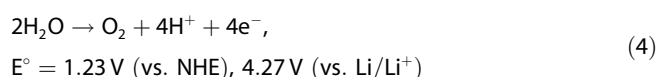
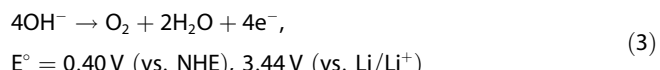


[a] Y. Bae,⁺ H. Park,⁺ Y. Ko,⁺ H. Kim,⁺ S. K. Park, Prof. K. Kang
Department of Materials Science and Engineering
Seoul National University
1 Gwanak-ro, Gwanak-gu, Seoul 151-742, Republic of Korea.
E-mail: matlgen1@snu.ac.kr

[b] Y. Bae,⁺ H. Park,⁺ Y. Ko,⁺ H. Kim,⁺ Prof. K. Kang
Center for Nanoparticle Research
Institute for Basic Science (IBS)
Seoul National University
1 Gwanak-ro, Gwanak-gu, Seoul 151-742, Republic of Korea.

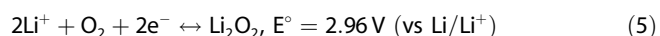
^{††} These authors contributed equally to this work
An invited contribution to a Special Issue on Bifunctional Catalysts for Metal-Air Batteries.

Under both basic and acidic conditions, the charge reaction takes place via the oxygen evolution reaction (OER) following Reaction (3) and (4), respectively.



The ORR and OER are proton-coupled four-electron transfer processes that involve $\text{O}=\text{O}$ bond breakage and formation, which result in sluggish kinetics and a high overpotential during the discharge/charge reaction in a $\text{Li}-\text{O}_2$ cell.^[13–15] Therefore, the development of bifunctional catalysts to enhance the kinetics of the ORR and OER is indispensable for the realization of aqueous $\text{Li}-\text{O}_2$ batteries.

On the other hand, non-aqueous $\text{Li}-\text{O}_2$ batteries are composed of Li metal, a non-aqueous electrolyte, and an air electrode in which discharge products of solid Li_2O_2 are produced and accumulated during discharge and decomposed during charge [Reaction (5)].

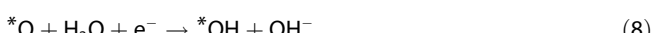
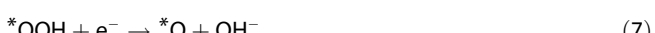
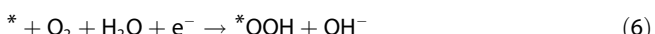


In non-aqueous $\text{Li}-\text{O}_2$ cells, the ORR and OER also occur, however, they are two-electron processes in which $\text{O}=\text{O}$ bonding is preserved during the reactions, resulting in relatively facile electron transfer kinetics, as demonstrated by density functional theory (DFT) calculations.^[16] However, the cycling of a non-aqueous $\text{Li}-\text{O}_2$ cell induces a considerable overpotential during both the ORR and OER; bifunctional catalysts are thus required to address this issue. Since the origin of the overpotential during the ORR and OER is distinct from that in the aqueous case, basic understanding of the origin of the overpotential is needed before the role of the catalyst can be discussed. Note that there presents the possibility of a consuming electron in unwanted side reaction resulting in the formation of a byproduct in both aqueous and non-aqueous systems, the accumulation of which causes the degradation of the cells. The management of byproduct formation

is also essential for a stable cycling of the cells, which is thoroughly discussed in recent literature.^[17–20] In the following, bifunctional catalysts for aqueous and non-aqueous $\text{Li}-\text{O}_2$ cells are introduced with explanations of the necessity and working mechanism of the catalysts.

2. Bifunctional Catalysts for Aqueous $\text{Li}-\text{O}_2$ Batteries

The detailed mechanism involving multistep electron-transfer processes during the ORR is generally described by the four steps in Reactions (6)–(9) in alkaline electrolyte, whereas the OER proceeds as the reverse reaction:^[21–24]



where * denotes a surface active site that adsorbs reactants and intermediates.

Because the ORR and OER occur at active sites of the catalyst surface, the activation barrier of each step is greatly affected by the adsorption energy of the oxygen-containing intermediate species. If the adsorption of the intermediate species is too strong, the desorption of the product becomes difficult, whereas with a weak adsorption of the intermediate species, the reactant is unlikely to adsorb on the active site. Thus, the catalytic activity can be higher with increasing adsorption energy to some point and descend after that point at which the change of rate-determining step occurs, which is well depicted by a typical volcano plot. Figure 1a and b present a volcano plot of several important catalysts reported, showing the trend of the catalytic activities for the ORR and OER, respectively, plotted against terms of the adsorption energies of the intermediate species.^[25] In each case,

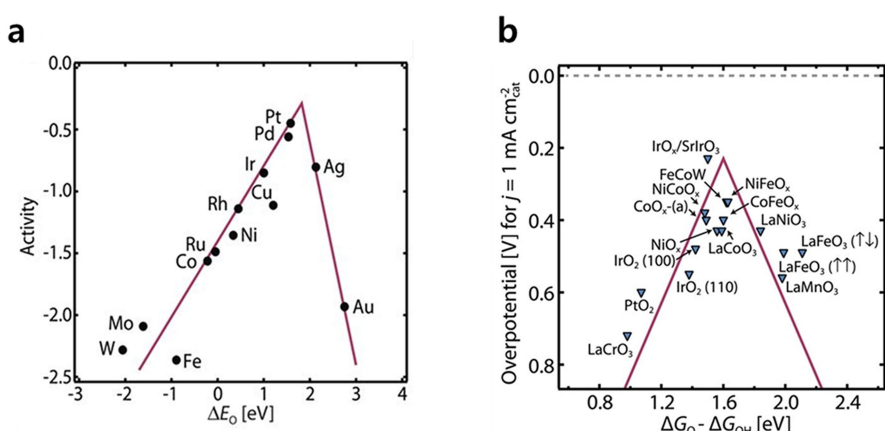


Figure 1. Volcano plots showing the trend in the catalytic activities for the (a) ORR and (b) OER based on DFT calculations and experimental data. Reprinted with permission. ref^[25] Copyright 2017, American Association for the Advancement of Science.

an adequate adsorption energy of the intermediate species leads to the best catalytic activities at the vertex of the volcano plot. In this respect, catalysts with suitable adsorption energy of the intermediate species are preferred to achieve a low activation barrier for each reaction and high ORR or OER activities. For bifunctional catalysts in aqueous Li–O₂ batteries, materials that possess catalytic activity for both the ORR and OER are required; thus, the adsorption energy of the intermediate species should be located near the vertices of both the ORR and OER volcano plots. Alternatively, a bifunctional catalyst can also be obtained by combining the separate ORR and OER catalysts into a composite material. According to the previous reports on the catalysts of aqueous Li–O₂ batteries, three groups of materials have been most extensively investigated as bifunctional catalysts; perovskite-type, spinel-type, and non-oxide catalysts. Although noble metals generally exhibit high catalytic activity for the ORR and OER, their high costs have limited their practical application, thus are excluded here.^[26,27] In the following sections, the catalytic activities of these three groups of materials in their applications to aqueous Li–O₂ batteries will be discussed.

2.1. Perovskite-Type Catalysts

Perovskite has the general formula of ABO₃, where the A sites are rare-earth metal ions and the B sites are transition metal ions. Suntivich et al. experimentally demonstrated the volcano-like trends of the OER and ORR catalytic properties of perovskites as a function of e_g orbital filling.^[28,29] They suggested that the OER and ORR properties are guided by the electron orbital of the transition metal because, based on the molecular orbital bonding framework, the occupancy of the transition metal e_g orbital determines the σ-bonding with the surface adsorbents. As the OER and ORR proceed via adsorption and desorption of the intermediate products, the binding energy of the surface adsorbents with the transition metal was believed to directly affect the kinetics of the reaction and consequently the performance of the catalyst. Specifically for the OER, the adsorption of OH[−] to *O resulting in *OOH (Reaction 7) were found to be the rate-determining step when e_g orbital filling is greater than 1, while the deprotonation of *OOH (Reaction 6) was found to be the rate-determining step when the e_g orbital filling is less than 1, which was revealed by the combination of experimental results and ab initio calculations.^[28] Thus, it was proposed that a catalyst with the e_g orbital filled with a single electron produces a desirable binding energy between the intermediate product and transition metal and exhibits the highest OER activity.^[28] They also showed that the catalytic properties of the ORR as well are strongly influenced by the e_g orbital, with the highest activity achieved when the orbital was filled with a single electron.^[29] These results indicate that a perovskite with a single-electron-filled e_g orbital can act as a bifunctional (both for OER and ORR) catalyst. Since there has been a recent report which demonstrated that the integrated ORR-OER may be significantly different from the cases of ORR-only or OER-only reaction because of the complicated issues such as operating voltage range, factors

affecting the efficiency of perovskite-type bifunctional catalysts should be further studied with more care.^[18]

Inspired by these finding, significant research efforts have focused on catalysts with the e_g orbital filled with a single electron.^[30–36] Cobalt-containing perovskites have been reported to be efficient bifunctional catalysts because the intermediate spin of Co³⁺ has an e_g orbital filled with one electron.^[33,34] Among cobalt-containing perovskite materials, Yang et al. observed that Sr_{0.95}Ce_{0.05}CoO_{3-δ} with copper nanoparticles as a conductive material was an efficient bifunctional catalyst.^[34] Figure 2a and b compare the discharge-charge voltage profiles and magnified discharge voltage profiles of hybrid Li–O₂ cells with various cathode materials, respectively. The cell with the carbon black (Vulcan XC-72) cathode exhibited a large voltage gap between discharge and charge, which resulted from the sluggish kinetics with proton-coupled four-electron transfer processes. In contrast, the cells with Sr_{0.95}Ce_{0.05}CoO_{3-δ} catalysts exhibited slightly reduced discharge overpotential, as observed in Figure 2b, and distinctly reduced charge overpotential, similar to the performance of noble metals (50% Pt/C). These results indicate the bifunctional catalytic activity of Co³⁺-based perovskite materials in hybrid Li–O₂ batteries. Nevertheless, the actual catalytic activity of the perovskite catalyst during the discharge process was inferior to that of a Pt/C catalyst, as observed in Figure 2b.

To further improve the ORR performance of perovskite catalysts, a composite bifunctional catalyst made of a perovskite material and N-doped carbon nanotube (NCNT), which is well known to be an efficient ORR catalyst, was developed.^[35,37] Park et al. synthesized a La_{0.5}Sr_{0.5}Co_{0.8}Fe_{0.2}O₃ perovskite nanoparticle (LSCF-NP) by calcination; then, a NCNT was directly grown on the surface of the LSCF-NP using chemical vapor deposition.^[35] As a result, an NCNT-wrapped LSCF-NP perovskite catalyst (op-LN) was successfully prepared, as shown in the scanning electron microscopy (SEM) images in Figure 2c. Cathodic linear sweep voltammetry (LSV) curves of LSCF-NP, Pt/C, NCNT, and op-LN catalysts were presented to compare the ORR activities of these catalysts (Figure 2d and e). It was demonstrated that the ORR activity was greatly increased with the help of the outer NCNT (Figure 2d) compared with the pristine LSCF-NP and was comparable to that of a state-of-the-art Pt/C catalyst (Figure 2e). It was also found that the OER activity of LSCF-NP could be improved with the surrounding NCNT, resulting in superior OER activity similar to that of a state-of-the-art Ir/C catalyst (Figure 2f). The increase in the OER activity with the NCNT was attributed to the facilitated charge transfer achieved owing to the conductive pathway provided by the surrounding NCNT. LSCF-NP with the ORR-active and conductive NCNT (op-LN) was accordingly tested as a bifunctional catalyst in a hybrid Li–O₂ battery. As shown in Figure 2g, the combined op-LN displayed the lowest discharge–charge voltage gap of 0.95 V at a current density of 0.5 mA cm^{−2}, which confirmed the bifunctional activity of the op-LN catalyst. At a current density of 0.2 mA cm^{−2}, op-LN could display impressively high bifunctional catalytic activity, resulting in a voltage gap of ~0.5 V in Figure 2h. Following this research, similar approaches were taken for various perovskite catalyst composites such as Nd_{0.5}Sr_{0.5}CoO_{3-δ}/conductive iodinated graphene nanoplatelets and La_{0.6}Sr_{0.4}Co_{0.2}Fe_{0.8}O_{3-δ}/palla-

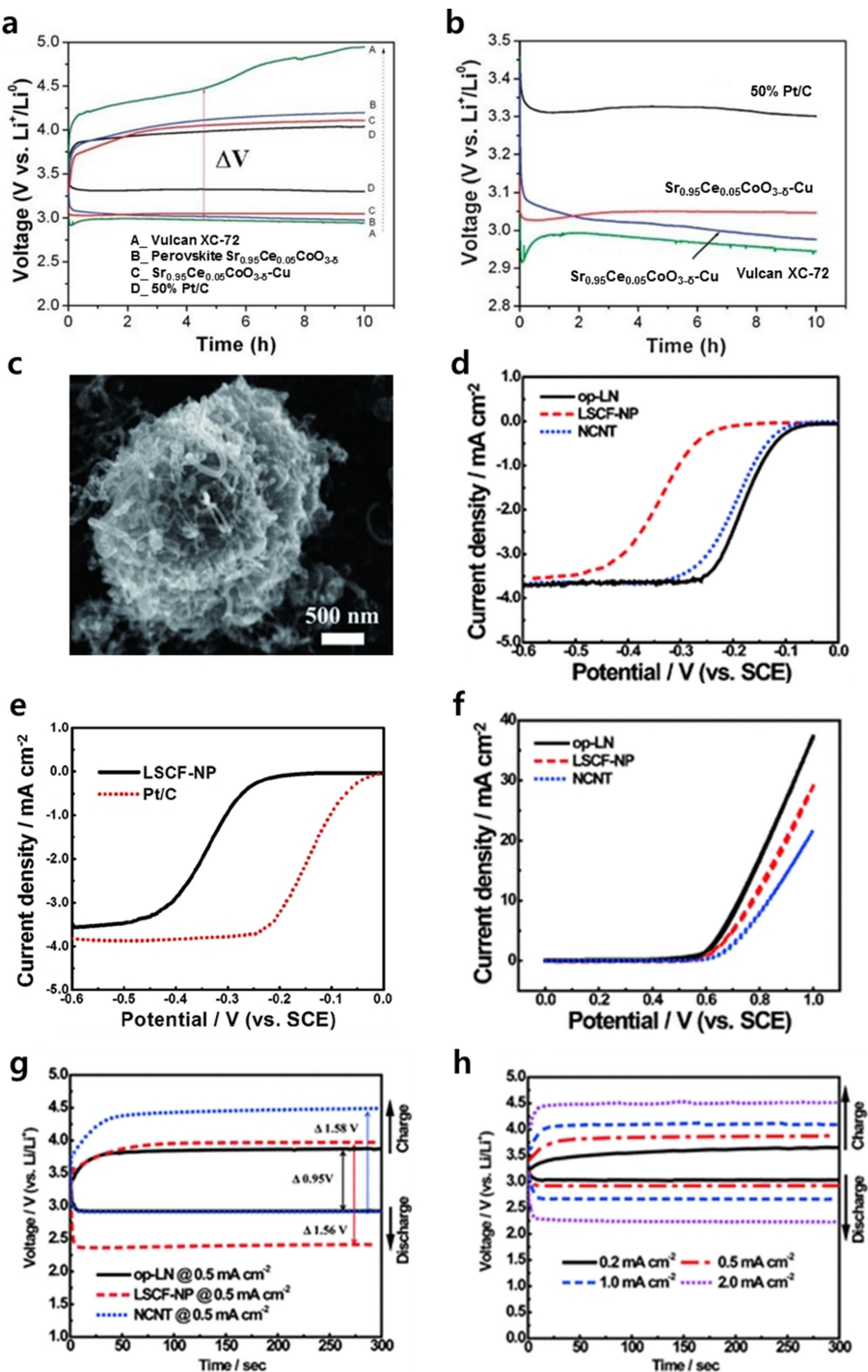


Figure 2. a) First discharge and charge curve of Vulcan carbon, Sr_{0.95}Ce_{0.05}CoO_{3-δ} catalysts, and Pt/C in hybrid Li–O₂ cells and b) magnified discharge curves. c) SEM image of op-LN. ORR polarization curves of d) op-LN, LSCF-NP/Vulcan carbon, and NCNT, e) LSCF-NP/Vulcan carbon and Pt/C obtained at a rotation speed of 900 rpm and scan rate of 10 mV s⁻¹ in O₂-saturated 0.1 M KOH solution. f) OER polarization curves of op-LN, LSCF-NP/Vulcan carbon, and NCNT obtained at a rotation speed of 900 rpm and scan rate of 10 mV s⁻¹ in O₂-saturated 0.1 M KOH solution. g) Discharge and charge polarization curve of op-LN, LSCF-NP, and NCNT in hybrid Li–O₂ cells. h) Discharge and charge polarization curve of op-LN at various current densities. Reprinted with permission from: a), b) ref. [34] Copyright 2012, Royal Society of Chemistry; c)-h) ref. [35] Copyright 2015, Wiley-VCH.

dium nanoparticles for improved ORR/OER activities in Li–O₂ batteries.^[36,38]

2.2. Spinel-Type Catalysts

Spinel-type catalysts have been also widely investigated as promising bifunctional catalysts.^[39–42] The general formula of a spinel material is AB₂O₄, where A is the element occupying

tetrahedral sites normally charged to 2+ and B is the one that takes up octahedral sites charged to 3+. The most intensively studied spinel-type catalysts include Co_3O_4 as bifunctional catalyst with the high activity.^[43] As Co exists in both 2+ and 3+ states, studies on the role of each state have been conducted. It was claimed that Co^{3+} at the octahedral sites are catalytically active for the OER.^[44,45] The catalytic role of Co^{3+} in the OER was determined in the comparative study of Co_3O_4 with ZnCo_2O_4 , considering that Zn^{2+} in the tetrahedral sites in ZnCo_2O_4 is catalytically inactive while Co^{3+} being in the octahedral sites.^[44,45] By comparing their catalytic activities, it was found that Co_3O_4 and ZnCo_2O_4 exhibited similar OER activities, suggesting that Co^{3+} at the octahedral site acts as the active site for the OER.^[44,45] It was also proposed that the high OER activity of Co^{3+} results from the intermediate spin Co^{3+} (e_g1) formed on the surface under OER conditions instead of the low-spin Co^{3+} (e_g0) configuration.^[45] Similar to the discussions made for perovskite materials,^[28] the e_g orbital filled with a single electron was believed to provide a desirable adsorption and desorption of OER intermediates, offering the high OER activity. However, for ORR, there are alternative views about the active site in spinel Co_3O_4 . Wei et al. proposed octahedral Co^{3+} as the active site for ORR based on single electron-filled e_g orbital interpretation, similar to the case of perovskite materials.^[46] On the other hand, Xiao et al. reported Co^{2+} as the active site for ORR since they found a correlation between higher Co^{2+} density and the improved ORR activity.^[47] They argued that when O_2 molecules are adsorbed on the active sites, the surface Co^{2+} ($3d^54s^2$) sites prefer to transfer electrons to the adsorbed O_2 molecules to weaken and break the $\text{O}=\text{O}$ bond while leaving themselves oxidized to Co^{3+} . These studies indicate that the bifunctionality of spinel Co_3O_4 is attributed to the synergistic effect of Co^{3+} and Co^{2+} , but further study is needed to reveal their precise role.

The bifunctional catalytic activities of Co_3O_4 /carbon composites were examined in aqueous $\text{Li}-\text{O}_2$ batteries.^[48–50] Sun et al. reported that the graphene- Co_3O_4 nanocomposite (Figure 3a) exhibited an onset potential of -0.11 V vs. the standard calomel electrode (SCE), which was 0.2- and 0.1-V higher than those of the commercial Co_3O_4 and pristine graphene, respectively (Figure 3b).^[48] In addition, the half-wave potential was greater than those of graphene and Co_3O_4 , indicating the enhanced ORR activity of the nanocomposite. At a current density of 1.5 mA cm^{-2} , the graphene- Co_3O_4 nanocomposite exhibited a potential of 0.65 V (vs. SCE) in the anodic LSV curves, further demonstrating the high OER activity (Figure 3c). These high bifunctional catalytic effects on the ORR/OER of the graphene- Co_3O_4 nanocomposite resulted not only from the intrinsic activity of the Co_3O_4 but also from the graphene, which compensated for the relatively low electrical conductivity of Co_3O_4 .^[51] Accordingly, the hybrid $\text{Li}-\text{O}_2$ cell employing the graphene- Co_3O_4 catalysts demonstrated a low polarization between the discharge and charge voltages (ΔV), which was substantially smaller than those for commercial carbon black or the pristine Co_3O_4 (Figure 3d). Because of the reduced ORR/OER overpotential, the aqueous $\text{Li}-\text{O}_2$ cell with the graphene- Co_3O_4 nanocomposite operated stably for over 50 cycles. Similarly,

CoMn_2O_4 nanoparticles, which could show high activity for the ORR and OER,^[43] were grown on the surface of graphene sheets (CMOG), as shown in Figure 3e.^[50] The highly active bifunctional catalyst combined with conductive graphene sheets was then applied as the cathode material in a hybrid $\text{Li}-\text{O}_2$ cell, resulting in only a 0.3 V gap between the discharge and charge potential at a current density of 0.025 mA cm^{-2} , as shown in Figure 3f. In addition to carbon materials, copper nanoparticles have also been used as conducting materials to achieve high catalytic activity of flower-like Co_3O_4 microspheres.^[49]

2.3. Non-Oxide Catalysts

Bifunctional catalysts for both ORR and OER can be categorized into two group: metal oxide-based catalysts such as perovskite and spinel, as discussed in the previous section, and non-oxide catalysts. Non-oxide catalysts are composed of carbon-based catalysts, metal hydroxide, metal sulfide, and so on.^[52–59] Among them, carbon based materials have been recently investigated as versatile and inexpensive alternatives for ORR or OER catalysts in the $\text{Li}-\text{O}_2$ batteries.^[54,60–64] Specifically, Fe–N-doped carbon (Fe–N–C) catalysts have been extensively studied and reported to be efficient ORR catalysts.^[65–68] Singh et al. proposed that the N-coordinated iron structure of FeN_x ($2 < x < 4$) is associated with the ORR reaction,^[66] whereas Strickland et al. reported that the N-doped carbon surface exhibits ORR activity and the $\text{Fe}/\text{Fe}_{x}\text{C}$ particulate stabilizes the peroxide intermediate on the active site.^[67] For OER, oxygen-functional-group-containing carbon materials have been observed to be efficient OER catalysts. The altered electronic structure of the adjacent carbon atoms was believed to result in facilitated adsorption of OER intermediates.^[69] Ji et al. exploited the Fe–N–C structure and O-doped carbon structure in a hierarchical 3D porous structure of a carbon fiber film with Fe, N, and O doping and surrounding CNT (FeNO–CNT–CNFF) to achieve bifunctional catalytic activity in an aqueous $\text{Li}-\text{O}_2$ battery, as shown in Figure 4a.^[54] The synthesized FeNO–CNT–CNFF contained fibers of ~ 600 -nm diameter covered by peapod-like CNTs (Figure 4b). This structure not only contained sufficient reaction sites on the external peapod-like CNTs but also provided efficient mass transport through the 3D hierarchical architecture. The catalytic activities of the Fe–N–C structure for the ORR and of the O-doped CNT for the OER in FeNO–CNT–CNFF were found to be better than those of Pt/C and Ir/C, respectively, in the LSV curve (Figure 4c). Figure 4d shows the high activity of the FeNO–CNT–CNFF catalyst used in a hybrid $\text{Li}-\text{O}_2$ cell. The cell exhibited a remarkably low voltage gap of 0.15 V between discharge and charge at a current density of 0.03 mA cm^{-2} , which was much lower than that of the Pt/C+Ir/C cathode ($\Delta V = 0.43$ V).

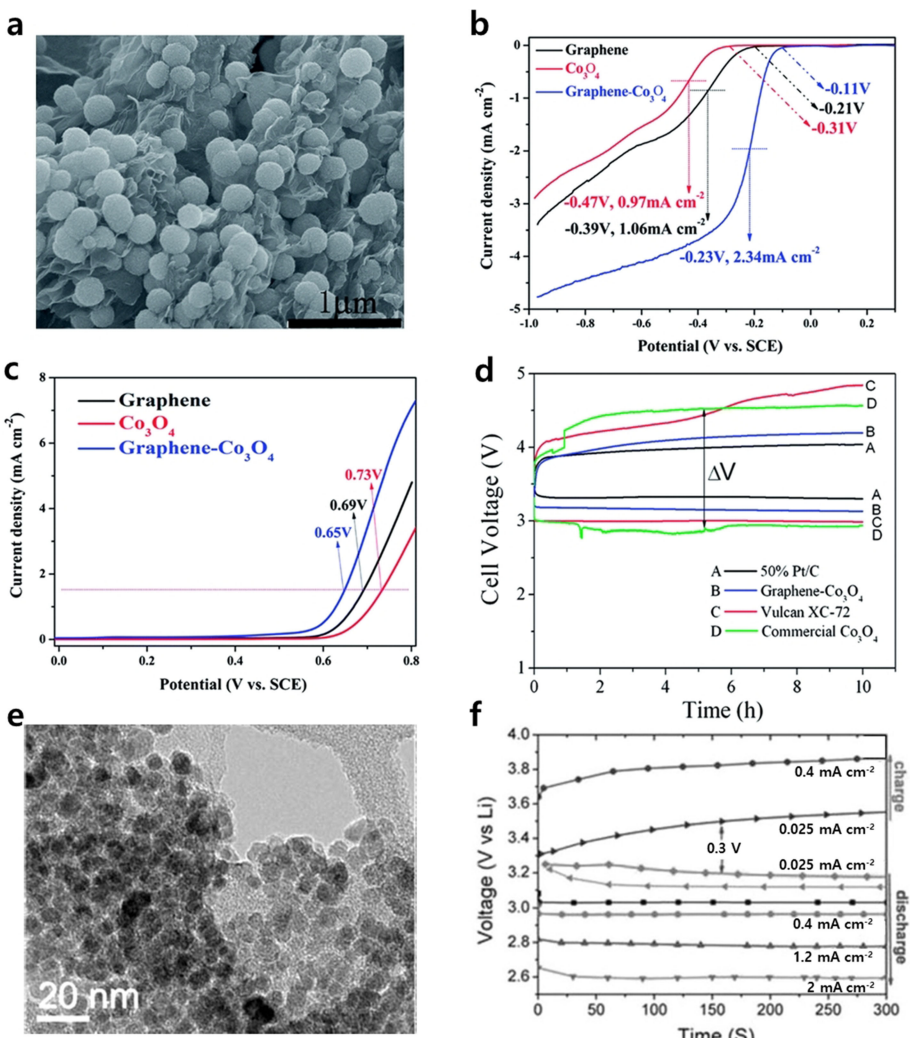


Figure 3. a) SEM images of as-prepared graphene-Co₃O₄. b) ORR polarization curves of graphene-Co₃O₄ composite, commercial Co₃O₄, and pristine graphene at a scan rate of 10 mV s⁻¹ and rotation speed of 1600 rpm in O₂-saturated 0.1 M KOH solution. c) Oxygen evolution currents of the different catalysts measured in Ar-saturated 0.1 M KOH solution at a scan rate of 80 mV s⁻¹. d) Comparison of first discharge and charge curves of the hybrid Li–O₂ batteries prepared with various catalysts at a current density of 80 mA g⁻¹. e) TEM image of CMOG. f) Voltage profiles at different current density of hybrid Li–O₂ cell with CMOG. Reprinted with permission from: a)–d) ref. [48] Copyright 2014, Royal Society of Chemistry; e), f) ref. [50] Copyright 2011, The Electrochemical Society.

3. Bifunctional Catalysts for Non-Aqueous Li–O₂ Batteries

In the early stage of the development of non-aqueous Li–O₂ batteries, catalysts were most extensively searched among noble-metal- or metal-oxide-based solid catalysts derived from well-established fields such as the fuel-cell and water-splitting systems. For example, various noble metals^[70–74] including Pt, Pd, Ru and Au, and metal oxides^[75–77] such as MnO₂, RuO₂, and Co₃O₄, which had successfully worked in aqueous systems, were introduced as catalysts for non-aqueous Li–O₂ batteries. Although enhanced electrochemical performance has been reported using these noble metals and metal oxides, controversies still remain regarding their working mechanism and the reversibility of the catalyst-assisted discharge/charge reaction.^[70–72,78]

Considering the distinct nature of the ORR (or OER) in aqueous and non-aqueous environments, the role of catalysts in non-

aqueous Li–O₂ batteries is understood to be different from those in aqueous media. As discussed in the previous section, the ORR and OER are accompanied by bond breakage and formation between two oxygen atoms, respectively, in aqueous media, which are associated with sluggish electron transfer kinetics. However, the ORR and OER in non-aqueous systems do not necessarily involve bond breaking of oxygen molecules. Accordingly, the electrocatalysts used in the aqueous system for the ORR and OER may not work for the non-aqueous Li–O₂ batteries,^[79] moreover, the conventional platform for measurement of the catalytic activity such as LSV in aqueous media is not sufficient to explain the enhanced electrochemical performance achieved with the use of a catalyst in a non-aqueous Li–O₂ battery.^[80–86] Nevertheless, the use of some solid catalysts has been reported to be advantageous for improving the electrochemical performance of non-aqueous Li–O₂ batteries, and their role can be elaborated based on an understanding of the different origin of the

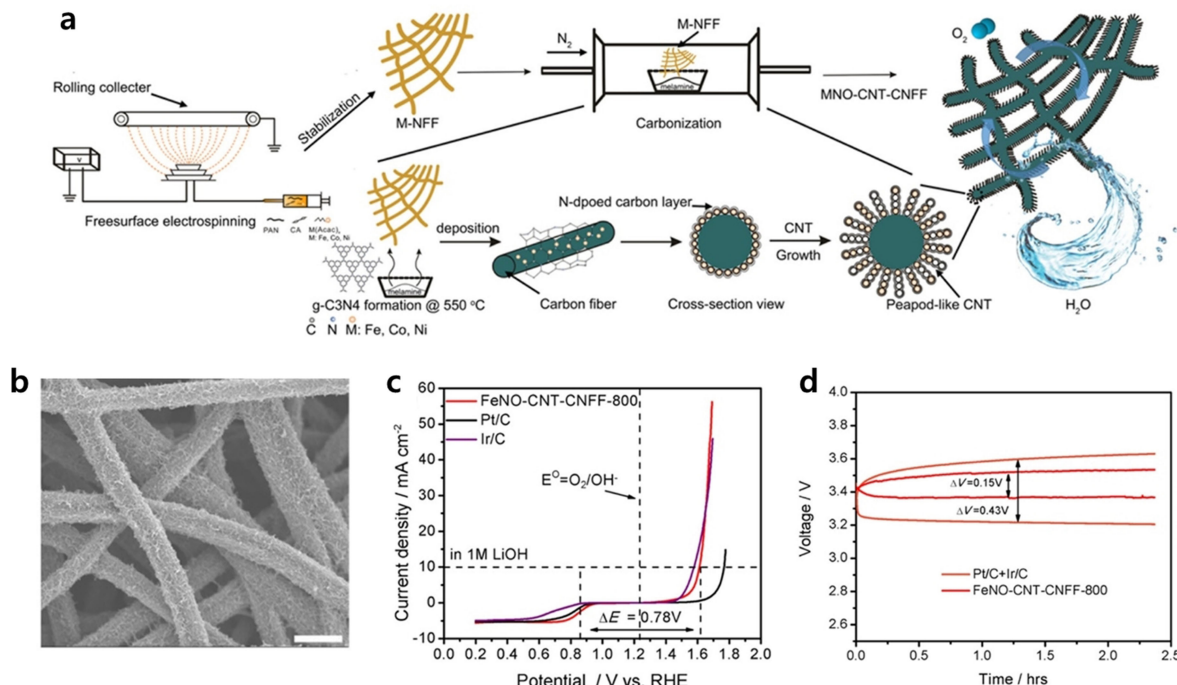


Figure 4. a) Schematic illustration of the fabrication process of FeNO-CNT-CNFFs. b) SEM images of FeNO-CNT-CNFF, scale bar: 1 μm. c) LSV curve of FeNO-CNT-CNFF, Pt/C, and Ir/C in 1 M LiOH at 1600 rpm. d) Comparison of voltage gap between discharge-charge voltage plateaus of hybrid Li-air batteries with FeNO-CNT-CNFF and Pt/C + Ir/C catalysts. Reprinted with permission from: a)–d) ref. [54] Copyright 2017 American Chemical Society.

overpotential. The theoretical voltage of Li_2O_2 formation from elemental lithium and oxygen gas (Reaction 5) is 2.96 V (vs. Li/Li^+); thus, a deviation of the discharge/charge voltage from 2.96 V is considered the overpotential. During discharge, the electrochemical reaction that determines the output voltage is either Reaction (10) or Reaction (11), the voltage of which is approximately 2.5–2.7 V (vs. Li/Li^+).^[87–89] It suggests that the overpotential during discharge may result not only from the sluggish kinetics but from the distinct electrochemical reduction path.



During charge, the electrochemical reaction determining the output charge voltage is the reverse reaction of Reaction 5. While the overpotential of the charge may come from the sluggish reaction of intrinsic OER,^[16] the low electrical conductivity of Li_2O_2 discharge product can also simply cause the IR drop resulting in the high polarization.^[90] It implies that the modification of the electrical properties of discharge products would contribute to reducing the overpotential. Based on these, it is clear that the term “catalyst” must be redefined more widely because the catalysts in this circumstance can reduce the overpotential in the ways other than how the conventional electrocatalyst could aid in the OER or ORR reactions. Generally, any material that enhances the electrochemical performance (e.g., polarization) is termed a catalyst in the non-aqueous $\text{Li}-\text{O}_2$ battery field. In the following, the catalysts for non-aqueous $\text{Li}-\text{O}_2$ batteries are categorized into

two groups depending on the phase of the material (i.e., solid-type and soluble-type bifunctional catalysts): metal- or metal-oxide-based solid catalysts, which are usually embedded in an air electrode as nanoparticles, and organic or halide-based soluble catalysts dissolved in an electrolyte.

3.1. Solid-Type Bifunctional Catalysts for Non-Aqueous $\text{Li}-\text{O}_2$ Batteries

Noble metals and their oxides have been most conventionally studied as catalysts in the early research of non-aqueous $\text{Li}-\text{O}_2$ batteries, focusing on the atomistic binding nature of the catalysts. It was reported that the oxygen binding energy on noble metal surfaces forms volcano-type trends with the ORR activity (i.e., discharge voltage), which is similar to the behavior observed in the aqueous case. Based on this observation, Pd and Pt were shown to exhibit the highest ORR catalytic activity owing to the adequate oxygen binding energy.^[74,91] However, the bifunctional catalytic activity in the non-aqueous systems was often demonstrated by regulating the property of the intermediate species, LiO_2 , thus the subsequent charge and discharge kinetics are influenced. In this case, the catalyst does not decrease the discharge or charge overpotential directly but rather modifies the property of the final discharge product, thereby reducing the subsequent charging overpotential. For example, Yilmaz et al. and Yang et al. reported that metal oxides such as RuO_2 and CeO_2 are capable of inducing the formation of film-like Li_2O_2 during discharge (Figure 5a). It was claimed that it is due to the increased affinity of the metal oxide surface

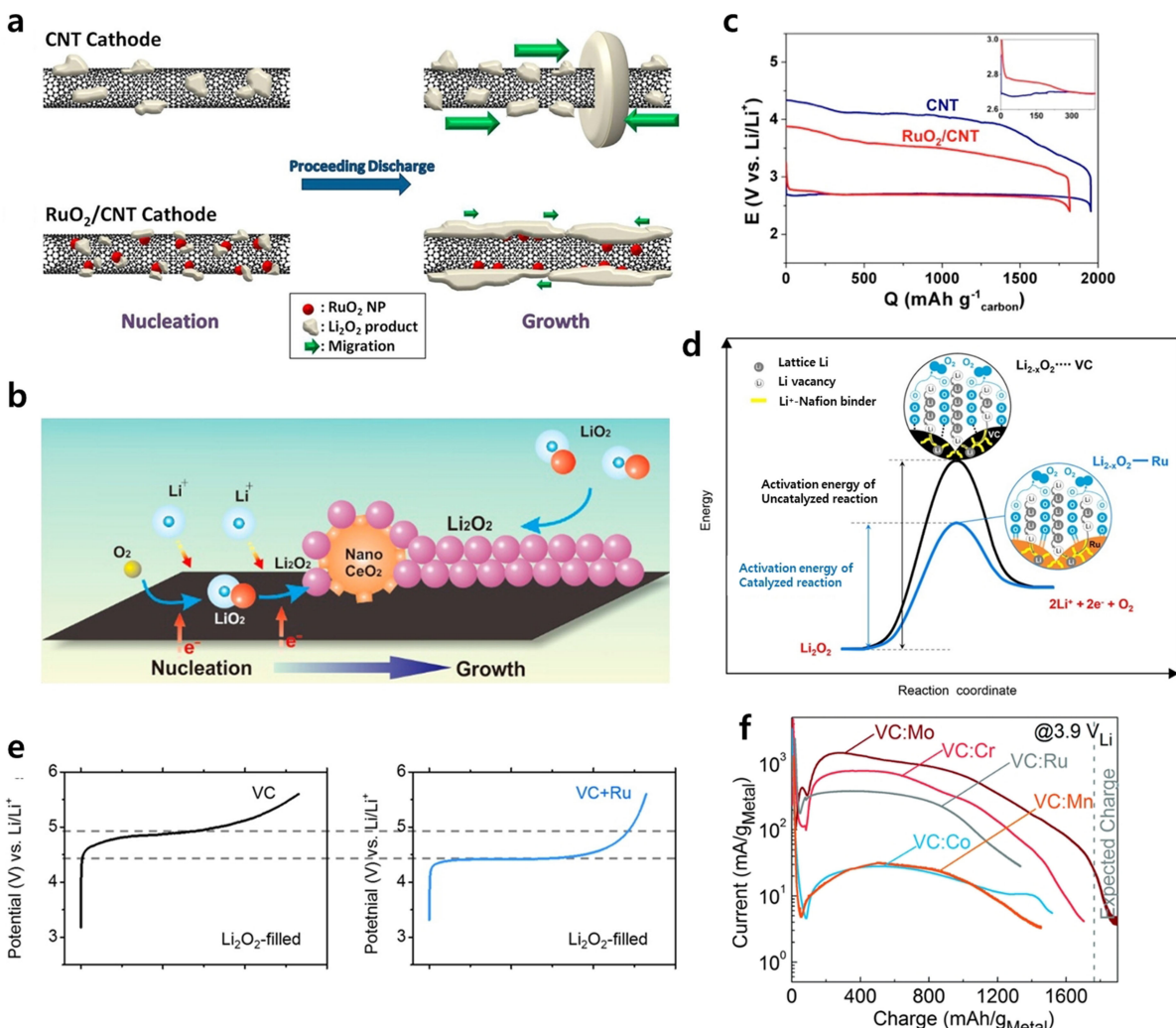


Figure 5. a) Schematic illustration of Li_2O_2 formation process in CNT and RuO_2/CNT cathodes. b) Schematic illustration showing CeO_2 -assisted formation of film-like Li_2O_2 . c) Discharge/recharge profiles of $\text{Li}-\text{O}_2$ cells with RuO_2/CNT (red) and CNT (blue) cathodes. d) Schematic illustration of Ru-catalyzed decomposition of Li_2O_2 by catalytic effect at solid interface between Ru and Li_2O_2 . e) Charge profile of Li_2O_2 -filled (left) carbon electrode and (right) Ru/carbon electrode. f) Current behavior of Li_2O_2 /metal/carbon composite electrode normalized by mass of metal. Reprinted with permission from: a) and c) ref. [92] Copyright 2013 American Chemical Society; b) ref. [93] Copyright 2016, American Chemical Society; d)–e) ref. [95] Copyright 2016 American Chemical Society; f) ref. [102] Copyright 2015 Royal Society of Chemistry.

toward intermediate species (Figure 5b).^[92,93] The intermediate species, LiO_2 [Reaction (10)], were speculated to be present as an adsorbed form on the surface of the catalyst long enough to undergo further electrochemical reduction [Reaction (11)], which results in the formation of film-like Li_2O_2 .^[87] The formation of film-like Li_2O_2 is advantageous in the subsequent charge process because of the increased electrical conductivity resulting from its amorphous property, as shown in Figure 5c.^[94] Thus, the charge overpotential could be substantially reduced with the aid of the catalyst working in the discharge process.

Some catalysts are more directly involved in the charge process. Wang et al. showed that Ru can catalyze the electrochemical formation of Li vacancies via solid-solid interaction at the Ru/ Li_2O_2 interface, which is followed by the facile electrochemical decomposition of $\text{Li}_{2-x}\text{O}_2$ (Figure 5d and e).^[95] It was found that generating Li vacancies in the Li_2O_2 structure via the formation of $\text{Li}_{2-x}\text{O}_2$ could lead to the increase in the charge

transport kinetics in the discharge product. Li vacancies in Li_2O_2 can also be generated by introducing dopants such as Co, Ni, and Si.^[96,97] Radin et al. demonstrated that Co-doped lithium peroxide, $\text{Li}_{2-x}\text{Co}_x\text{O}_2$, exhibited remarkably enhanced charge-transport properties and could be decomposed at lower potential compared with Li_2O_2 .^[96] They reported that when Co_3O_4 nanoparticles were used as a catalyst, Co^{2+} ions dissolved from cobalt oxide were impregnated into Li_2O_2 to form $\text{Li}_{2-x}\text{Co}_x\text{O}_2$. This idea was supported by subsequent research papers reporting the enhanced electrochemical performance of Co_3O_4 -embedded $\text{Li}-\text{O}_2$ batteries.^[98–101] The conversion of Li_2O_2 with metal- and metal-oxide-based catalysts has also been suggested to increase the oxidation kinetics of Li_2O_2 . Yao et al. reported that various metals (Cr, Mo, and Ru) and their oxides enhanced the charge kinetics of a $\text{Li}-\text{O}_2$ battery by converting Li_2O_2 into the intermediate $\text{Li}_x\text{M}_y\text{O}_z$ phase, which has faster kinetics of de-lithiation than Li_2O_2 (Figure 5f).^[102]

The distinct role of the catalyst in non-aqueous systems proposes that the definition of a bifunctional catalyst for non-aqueous Li–O₂ batteries must be different from that for the aqueous case, where catalysts that reduce the activation energy of both the forward (i.e., oxygen reduction) and backward (i.e., oxygen evolution) electrochemical reaction are considered “bifunctional”. In a non-aqueous system, catalysts that result in reduced polarization by functioning in the ways elaborated above during discharge and charge can be regarded as bifunctional. In this respect, Ru-based catalysts (Ru and RuO₂) are the most representative case of bifunctional catalysts for non-aqueous Li–O₂ batteries, as they induce the formation of film-like Li₂O₂ during discharge^[92] and promote the generation of Li_{2-x}O₂ during charge.^[95] It is noteworthy that not only a reduction in polarization, but also a reversibility of catalyzed reactions needs to be investigated for more precise evaluation on the catalytic activity. For example, a quantitative analysis such as discharge product titration and gas evolution measurement during charge process can be an indicator for a true activity of catalysts.

While solid catalysts have been demonstrated to be beneficial in improving the electrochemical performance in many studies, the intrinsic interfacial nature between the solid catalyst and solid product of Li₂O₂ still presents a great hurdle. The principal reaction of non-aqueous Li–O₂ batteries is gas-to-solid phase transformation, which inevitably results in a solid-solid interface between the catalyst and discharge product, whereas the catalysts for an aqueous system can conserve the solid-to-liquid interface because of the soluble nature of all the reactants, intermediate and products. During the initial stage of discharge of non-aqueous Li–O₂ batteries, the exposed catalytic surfaces are capable of efficiently promoting the reduction reaction of the gas phase or dissolved oxygen; nevertheless, the deposition of solid products gradually covers the surfaces of the active catalysts as discharge continues until, finally, all the active surfaces of the solid catalysts are passivated by insulating discharge products.^[103–106] Once passivated, the catalysts are expected to lose their functionality for further discharge reactions, which is similar to the “deactivation” or “poisoning” phenomena observed in various catalyst application fields.^[107–110] Analogously, bifunctional catalysts can facilitate the OER for Li₂O₂ in direct contact with the catalyst during the charge process; however, the OER functionality for Li₂O₂ not in a direct contact with the catalyst remains doubtful and controversial because of the inefficiency of the solid-solid interface.

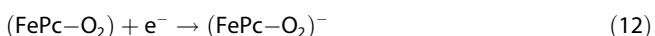
3.2. Soluble-Type Bifunctional Catalyst for Non-Aqueous Li–O₂ Batteries

Because of the intrinsic limitation of solid catalysts regarding the reaction interface, recent studies have focused on the evolution of soluble and mobile catalysts to catalyze the solid discharge products in conventional non-aqueous Li–O₂ batteries. The concept of soluble catalysts is that a species that is dissolved in an electrolyte and thus freely moves around drives the catalytic reaction sites into the electrolyte solution rather than to the surface of the electrode or solid catalysts. Many different types of soluble catalysts have been proposed,

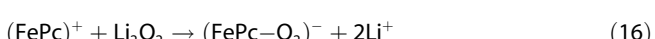
including organic redox-active species (e.g., organosulfur,^[111–114] nitroxyl radical,^[115–121] phenazine,^[122–124] quinone^[125–130] and halide (e.g., iodide^[131–142], bromide^[143,144]) as well as organometallic compounds (e.g., phthalocyanine,^[145,146] protoporphyrin^[147]).

Such soluble catalysts can be categorized into an oxygen species carrier and a redox mediator depending on what the catalysts mediate. Oxygen-carrier molecules have been proposed to facilitate both the ORR and OER by shuttling oxygen species between the electrode and reaction products. The key property of oxygen-carrying catalysts is the effective adsorption of oxygen species (oxygen molecule, superoxide or peroxide) on the central metal ions of organometallic compounds. Iron phthalocyanine (FePc) was first suggested as a bifunctional soluble catalyst for non-aqueous Li–O₂ batteries, as shown in Figure 6a and b.^[146] The coordination of oxygen species with iron ions was evidenced by the red shift of the characteristic absorption bands of organometallic compounds using UV-vis spectroscopy (Figure 6c). During discharge, the strong interactions of the oxygen molecules with metal ions form [FePc–O₂] complexes, which subsequently combine with lithium ions after reduction, leading to the formation of [FePc–LiOOLi] complexes. It was suggested that the [FePc–LiOOLi] complexes diffuse to the Li₂O₂ nucleated sites, and then, the dissociated Li₂O₂ is incorporated into the crystal lattice with the recovery of the FePc soluble catalyst. Such solution-phase formation of Li₂O₂ was speculated to prevent the early passivation or clogging of the active surface, as confirmed by the current increase in cyclic voltammetry measurements and morphology examinations after discharge. For the recharge process, it was found that oxidized catalysts bind with any available reduced oxygen species from LiO₂ or Li₂O₂ in the solution phase and decompose it into a lithium ion and oxygen, as depicted in Figure 6b. The bifunctional catalytic activity of FePc was confirmed by the markedly reduced polarization for both discharge and charge of Li–O₂ cells, which resulted in the enhanced cycle stability up to 130 times compared with that of only 20 cycles without catalysts (Figure 6d). Similarly, a family of phthalocyanine compounds containing cobalt metal ions (tertbutyl cobalt phthalocyanine) has also been suggested to be an efficient soluble catalyst for non-aqueous Li–O₂ batteries.^[145] The reaction mechanisms of FePc during the ORR and OER are summarized by Reactions (12)–(17).

ORR:



OER:



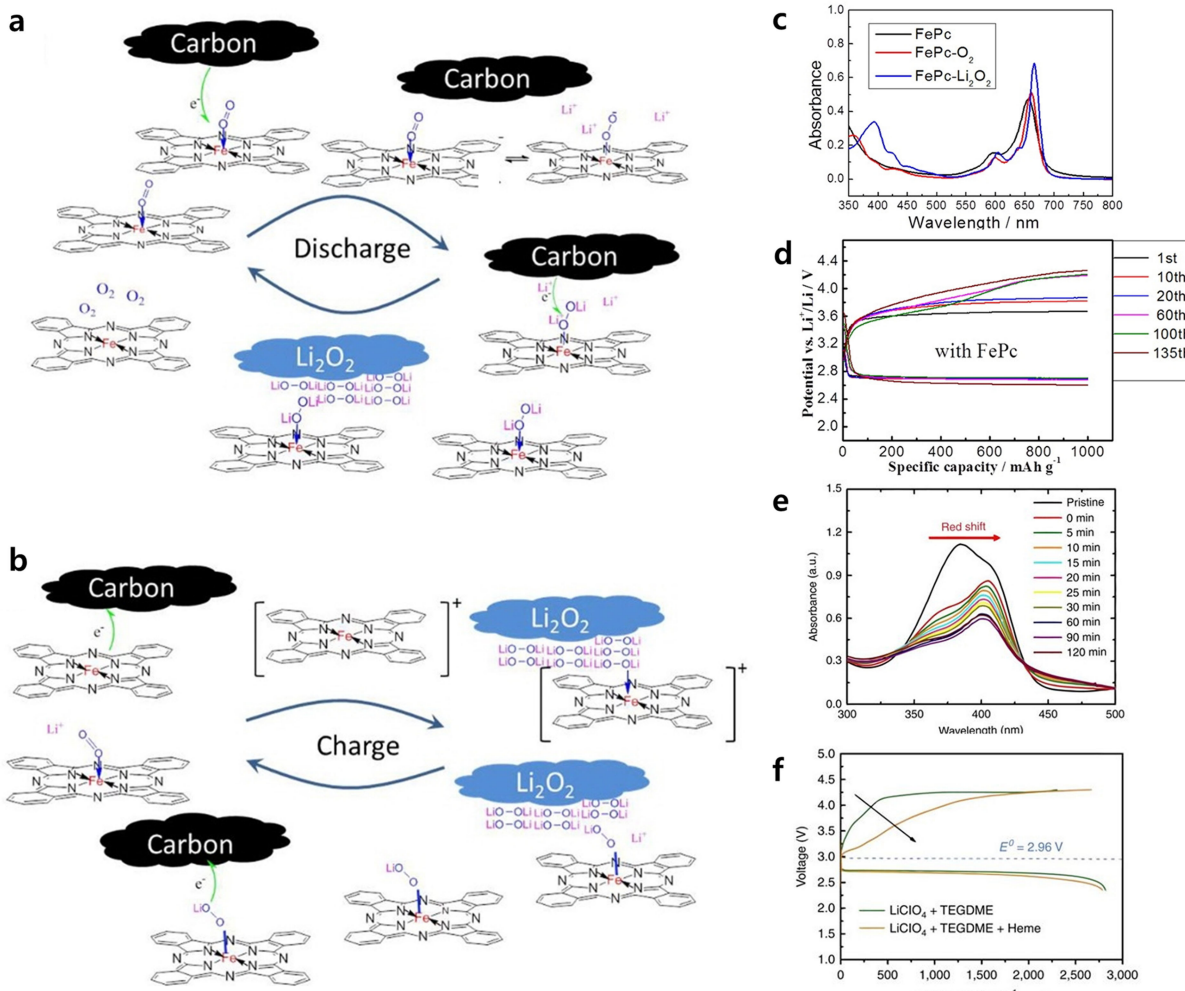


Figure 6. Schematic illustration of working mechanism of FePc soluble catalyst for a) discharge and b) charge reaction of Li–O₂ battery. c) Red shift of absorbance band of FePc in UV–vis spectra. d) Discharge/charge profiles of Li–O₂ battery with FePc catalysts. e) Red shift of absorbance band of heme in UV–vis spectra. f) Discharge/charge profile of Li–O₂ battery with heme catalysts. Reprinted with permission from: a)–d) ref. [146] Copyright 2014, American Chemical Society; e),f) ref. [147] Copyright 2016, Nature Publishing Group.

Ryu et al. exploited the bio-inspired organometallic biomolecule, an iron protoporphyrin (heme), as a bifunctional catalyst from the widely applied oxygen-shuttling properties of heme molecules.^[147] The coordination between the iron ion and superoxide moiety was supported by the red shifts of the characteristic absorption band of the heme molecule, as shown in Figure 6e. The reversibility of the oxygen shuttling behavior for the entire ORR and OER could be confirmed by in-situ spectro-electrochemical examinations. The efficient and reversible oxygen shuttling property of heme catalysts could lead to a significantly enhanced energy efficiency and cycling stability of Li–O₂ batteries (Figure 6f).

The working principle of a redox mediator, another type of soluble catalyst, is that the redox-active species electrochemically reacts before oxygen (for discharge) or Li₂O₂ (for charge) participates in the electrochemical reaction, and then, the reduced or oxidized species spontaneously reacts with oxygen (for discharge) or Li₂O₂ (for charge) based on the chemical driving force. Thus, it can ensure the efficient chemical conversion of

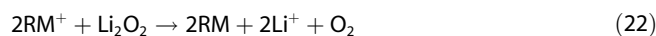
oxygen into Li₂O₂ in electrolyte solution and vice versa without going through the direct electrochemical reaction of Li₂O₂. The key merit is that the redox mediator can deliver electrons or holes to reaction sites far from the electrode, which is the reason this material is termed a redox mediator, and thus, the operation voltage of Li–O₂ batteries is determined by the redox potential of the mediator. In addition, the use of a redox mediator makes direct electron conduction through the insulating Li₂O₂ unnecessary, thus remarkably reducing the polarizations of Li–O₂ batteries, particularly for the charge process. The reaction mechanisms of the redox mediator during the ORR and OER are described by Reactions (18)–(22).

ORR redox mediation:





OER redox mediation:



Most redox mediators so far have been designed based on the thermodynamic potential difference, as depicted in Figure 7a and b,^[122,125,148] thus could be active for only one reaction, either the ORR or OER, rather than serving as a bifunctional catalyst. Although a few redox mediators, such as 2,6-di-tert-butyl-hydroxytoluene (BHT)^[149] and 2-phenyl-4,4,5,5-tetramethylimidazoline-1-oxyl-3-oxide (PTIO),^[119] have been reported as bifunctional soluble catalysts, the origin of the dual functionality as well as the detailed working mechanism are still not fully understood, which has to be further studied with precise examinations of efficacy for both the ORR and OER. On the other hand, dual functionality can be imparted simply by implementing two different catalysts dissolved in non-aqueous Li–O₂ batteries. Gao et al. reported a Li–O₂ battery containing both ORR and OER redox mediators, 2,5-di-tert-butyl-1,4-benzoquinone (DBBQ) and 2,2,6,6-tetramethyl-1-piperidinyloxy (TEMPO), respectively, as shown in Figure 7c.^[128] In the dual-mediator Li–O₂ battery, for which the surface electrochemistry only involves electron transfer between mediating molecules, the formation and decomposition of Li₂O₂ occur in electrolyte solutions rather than on the electrode surface, which greatly improves the cell capacity and reversibility, as shown in Figure 7d. The solution phase reaction has been demonstrated to prevent intimate contact of the carbon electrodes with Li₂O₂, which is also beneficial for mitigating the degradation of the carbon cathode by parasitic reactions, one of the major causes

of cycle deterioration for Li–O₂ batteries. This strategy can also provide design flexibility for cell systems such as redox-flow Li–O₂ batteries that use dual mediators, as shown in Figure 7e.^[150,151] More recently, Lee et al. proposed RuBr₃ as a hybrid bifunctional catalyst for Li–O₂ battery (Figure 7f).^[152] In the dissolved state of RuBr₃ catalyst, ruthenium ions function as an oxygen-carrying catalyst for the ORR, whereas bromide ions serve as typical halide OER redox mediator, resulting in significantly improved energy efficiency for both charge and discharge reactions.

Soluble catalysts are now regarded as a key to solving several intrinsic problems associated with conventional non-aqueous Li–O₂ batteries by offering a highly efficient solid-liquid interface. However, the diffusible nature of soluble catalysts inevitably results in shuttling phenomena or crossover between the anode and cathode, which share the same electrolyte in a non-aqueous Li–O₂ battery. Such shuttle behavior can significantly reduce the efficacy of soluble catalysts and even result in the continuous loss of catalysts owing to undesirable parasitic reactions with the lithium anode. The detrimental effects of shuttle phenomena have been demonstrated in several model studies in which interlayers such as inorganic solid electrolyte^[118] and advanced separator^[114,123] were introduced between the anode and cathode to selectively permit the penetration of mobile species. The introduction of protection layers on the lithium anode has also been proposed as a potential solution to prevent shuttle reactions.^[121,138] One of the recent promising strategies is controlling the mobility of redox mediators including precipitating redox mediators such as modified tetrathiafulvalene and polymerization of redox mediators (polyantraquinone).^[153,154] Nevertheless, as research on soluble catalysts remains in the early stage, it is believed that further community efforts are

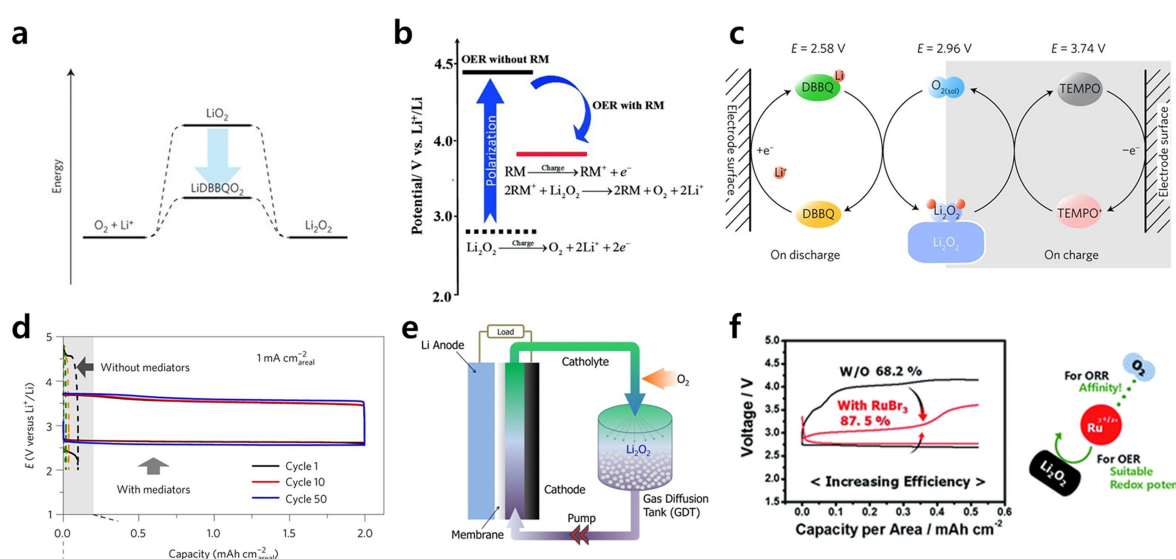


Figure 7. Graphical illustrations of thermodynamic potential relationship for a) ORR redox mediator and b) OER redox mediator. c) Schematics of a dual-mediating Li–O₂ battery. d) Discharge/charge profiles of Li–O₂ battery with dual mediators. e) Schematic illustrations of Li–O₂ redox-flow battery. f) Discharge/charge profiles of Li–O₂ battery with RuBr₃ soluble catalyst with graphical description of mechanism. Reprinted with permission from: a) ref. [125] Copyright 2016, Nature Publishing Group; b) ref. [148] Copyright 2015, Wiley-VCH Verlag GmbH & Co; c)-d) ref. [128] Copyright 2017, Nature Publishing Group; e) ref. [151] Copyright 2016, American Chemical Society; f) ref. [152] Copyright 2017, Royal Society of Chemistry.

Table 1. Summary on the performance of bifunctional catalysts in aqueous Li–O₂ batteries.

| Catalyst | Current Density | Discharge/Charge voltage difference (ΔV) | Round-trip efficiency | Reference No. |
|--|---|--|-----------------------|---------------|
| Vulcan XC-72 | 0.05 mA cm ⁻² | 1.51 V | 58.8 % | [34] |
| Sr _{0.95} Ce _{0.05} CoO _{3-δ} | 0.05 mA cm ⁻² | 1.11 V | 72.3 % | [34] |
| Sr _{0.95} Ce _{0.05} CoO _{3-δ} –Cu | 0.05 mA cm ⁻² | 0.98 V | 75.2 % | [34] |
| 50 % Pt/C | 0.05 mA cm ⁻² | 0.65 V | 83.0 % | [34] |
| op-LN | 0.2 mA cm ⁻² | 0.5 V | – | [35] |
| Graphene–Co ₃ O ₄ | 80 mA g ⁻¹ (0.025 mA cm ⁻²) | 0.97 V | 76.5 % | [48] |
| Graphene–CoMn ₂ O ₄ | 0.025 mA cm ⁻² | 0.3 V | – | [50] |
| FeNO–CNT–CNFF | 0.03 mA cm ⁻² | 0.15 V | – | [54] |
| 20 % Pt/C + 20 % Ir/C | 0.03 mA cm ⁻² | 0.43 V | – | [54] |

Table 2. Summary on catalysis mechanisms of various catalysts for non-aqueous Li–O₂ batteries.

| Catalyst type | Catalyzing reaction | Catalysis mechanism | Representative Catalysts | Reference No. |
|---------------|---------------------|---|--|---------------------------------|
| Solid type | ORR | Adjusting oxygen binding energy | Pd | [74] |
| | | Tuning the morphology of Li ₂ O ₂ into amorphous phase | Pt RuO ₂ CeO ₂ | [74] [92] [93] |
| | OER | Catalyzing the electrochemical formation of Li _{2-x} O ₂ phase | Ru | [95] |
| | | Generating Li vacancy by doping Converting Li ₂ O ₂ into Li _x M _y O ₂ phase | Co ₃ O ₄ Cr, Cr ₂ O ₃ Mo, MoO ₃ Ru, RuO ₂ | [96] [102] [102] [102] |
| Soluble type | ORR | Carrying oxygen species from electrode to Li ₂ O ₂ | FePc Heme | [146] [147] |
| | | Redox mediation (electron transfer to O ₂) | DBBQ | [125] |
| | OER | Carrying oxygen species from Li ₂ O ₂ to electrode | Vitamin K2 FePc Heme | [130] [146] [147] |
| | | Redox mediation (hole transfer to Li ₂ O ₂) | TTF Lil TEMPO | [111] [131] [115] |

needed for the efficient use of soluble catalysts in non-aqueous Li–O₂ batteries.

4. Summary

In this article, various bifunctional catalysts were reviewed, which have been employed in Li–O₂ batteries either in aqueous or non-aqueous systems. In aqueous systems, the ORR and OER are primarily limited in the proton-coupled four-electron transfer processes including O=O bond breakage and formation. Therefore, the use of bifunctional catalysts to reduce the activation barriers of the ORR and OER has been indispensable for the efficient operation of aqueous Li–O₂ batteries. Since the adsorption energy of the intermediate species is a critical factor determining the activation barrier of each reaction, a catalyst that offers an appropriate adsorption energy was important. Perovskite-type, spinel-type and non-oxide materials have been extensively used as bifunctional catalysts in aqueous Li–O₂ batteries because of their suitable electronic structure such as e_{g1} and the adequate adsorption energy of the intermediate species. In addition, rapid mass and electron transport around active sites of the catalysts were required for facile electrochemical reactions on catalyst materials. As a result, composite

materials of catalysts and conducting materials with a porous structure have been widely developed to enhance the mass and electron transport and further increase the ORR and OER activity. The performances of bifunctional catalysts in aqueous Li–O₂ batteries are summarized in Table 1. In non-aqueous Li–O₂ batteries, solid-type catalysts were typically designed to induce the formation of conductive amorphous Li₂O₂ during discharge and promote the facile decomposition of Li₂O₂ by enhancing the charge-transport properties. Solid-type catalysts could also aid in generating Li vacancies or converting Li₂O₂ into lithium metal oxide, thereby the decomposition reaction is kinetically enhanced. Soluble catalysts including two groups of oxygen-carriers and redox mediators have been recently introduced and shown to alter the surface electrochemistry of non-aqueous Li–O₂ batteries to solution-dominant electrochemistry. The solution-phase reaction has resulted in great enhancements of the energy efficiency and cycle reversibility of non-aqueous Li–O₂ batteries by circumventing the inefficient solid/solid interface issue; however, several issues originating from the diffusible nature of soluble catalysts remain unresolved, which prevent the realization of high-energy and efficient energy storage of Li–O₂ batteries. The summary on catalysis mechanisms of catalysts dealt in this paper for non-aqueous Li–O₂ batteries is presented in Table 2.

Acknowledgements

This work was supported by the World Premier Materials grant funded by the Korea government Ministry of Trade, Industry and Energy. We acknowledged the financial support by the National Research Foundation of Korea (NRF) grant funded by the Korea government (MSIP) (No. 2018R1A2A1A05079249). This work was also supported by Project Code. (IBS-R006-A2). This research was also supported by Creative Materials Discovery Program through the National Research Foundation of Korea (NRF) funded by the Ministry of Science, ICT and Future Planning (NRF-2017M3D1A1039553)

Conflict of Interest

The authors declare no conflict of interest.

Keywords: bifunctionality • electrocatalyst • lithium–oxygen batteries • oxygen electrochemistry • soluble catalyst

- [1] S. Chu, Y. Cui, N. Liu, *Nat. Mater.* **2016**, *16*, 16.
- [2] S. Park, Y. Shao, J. Liu, Y. Wang, *Energy Environ. Sci.* **2012**, *5*, 9331–9344.
- [3] H. Zhang, Z. Ma, J. Duan, H. Liu, G. Liu, T. Wang, K. Chang, M. Li, L. Shi, X. Meng, K. Wu, J. Ye, *ACS Nano* **2016**, *10*, 684–694.
- [4] B. Dunn, H. Kamath, J.-M. Tarascon, *Science* **2011**, *334*, 928–935.
- [5] J. Lu, L. Li, J.-B. Park, Y.-K. Sun, F. Wu, K. Amine, *Chem. Rev.* **2014**, *114*, 5611–5640.
- [6] P. G. Bruce, S. A. Freunberger, L. J. Hardwick, J.-M. Tarascon, *Nat. Mater.* **2011**, *11*, 19.
- [7] H.-D. Lim, B. Lee, Y. Bae, H. Park, Y. Ko, H. Kim, J. Kim, K. Kang, *Chem. Soc. Rev.* **2017**, *46*, 2873–2888.
- [8] A. Manthiram, Y. Fu, S.-H. Chung, C. Zu, Y.-S. Su, *Chem. Rev.* **2014**, *114*, 11751–11787.
- [9] A. Zhamu, G. Chen, C. Liu, D. Neff, Q. Fang, Z. Yu, W. Xiong, Y. Wang, X. Wang, B. Z. Jang, *Energy Environ. Sci.* **2012**, *5*, 5701–5707.
- [10] M. M. Thackeray, C. Wolverton, E. D. Isaacs, *Energy Environ. Sci.* **2012**, *5*, 7854–7863.
- [11] A. Manthiram, L. Li, *Adv. Energy Mater.* **2015**, *5*, 1401302.
- [12] R. Black, B. Adams, L. F. Nazar, *Adv. Energy Mater.* **2012**, *2*, 801–815.
- [13] F. Cheng, J. Chen, *Chem. Soc. Rev.* **2012**, *41*, 2172–2192.
- [14] N.-T. Suen, S.-F. Hung, Q. Quan, N. Zhang, Y.-J. Xu, H. M. Chen, *Chem. Soc. Rev.* **2017**, *46*, 337–365.
- [15] Y. Jiao, Y. Zheng, M. Jaroniec, S. Z. Qiao, *Chem. Soc. Rev.* **2015**, *44*, 2060–2086.
- [16] J. S. Hummelshøj, A. C. Luntz, J. K. Nørskov, *J. Chem. Phys.* **2013**, *138*, 034703.
- [17] Y. Liu, L. Wang, L. Cao, C. Shang, Z. Wang, H. Wang, L. He, J. Yang, H. Cheng, J. Li, *Mater. Chem. Front.* **2017**, *1*, 2495–2510.
- [18] L. Köhler, L. Szabadić, C. Jooss, M. Risch, *Batteries & Supercaps* **10.1002/batt.201800119**.
- [19] X. Shi, S. Siahrostami, G.-L. Li, Y. Zhang, P. Chakrhanont, F. Studt, T. F. Jaramillo, X. Zheng, J. K. Nørskov, *Nat. Commun.* **2017**, *8*, 701.
- [20] Z. Zhao, J. Huang, Z. Peng, *Angew. Chem. Int. Ed.* **2018**, *57*, 3874–3886; *Angew. Chem.* **2018**, *130*, 3936–3949.
- [21] Z. F. Huang, J. Wang, Y. Peng, C. Y. Jung, A. Fisher, X. Wang, *Adv. Energy Mater.* **2017**, *7*, 1700544.
- [22] H. Dau, C. Limberg, T. Reier, M. Risch, S. Roggan, P. Strasser, *ChemCatChem* **2010**, *2*, 724–761.
- [23] M. Bajdich, M. García-Mota, A. Vojvodic, J. K. Nørskov, A. T. Bell, *J. Am. Chem. Soc.* **2013**, *135*, 13521–13530.
- [24] H. Kim, J. Park, I. Park, K. Jin, S. E. Jerng, S. H. Kim, K. T. Nam, K. Kang, *Nat. Commun.* **2015**, *6*, 8253.
- [25] Z. W. Seh, J. Kibsgaard, C. F. Dickens, I. Chorkendorff, J. K. Nørskov, T. F. Jaramillo, *Science* **2017**, *355*, eaad4998.
- [26] Y. Lee, J. Suntivich, K. J. May, E. E. Perry, Y. Shao-Horn, *J. Phys. Chem. Lett.* **2012**, *3*, 399–404.
- [27] F. Lima, J. Zhang, M. Shao, K. Sasaki, M. Vukmirovic, E. Ticianelli, R. Adzic, *J. Phys. Chem. C* **2007**, *111*, 404–410.
- [28] J. Suntivich, K. J. May, H. A. Gasteiger, J. B. Goodenough, Y. Shao-Horn, *Science* **2011**, *334*, 1383–1385.
- [29] J. Suntivich, H. A. Gasteiger, N. Yabuuchi, H. Nakanishi, J. B. Goodenough, Y. Shao-Horn, *Nat. Chem.* **2011**, *3*, 546.
- [30] J. Bian, R. Su, Y. Yao, J. Wang, J. Zhou, F. Li, Z. Wang, C. Sun, *ACS Appl. Energy Mater.* **2019**.
- [31] Y. Yamada, K. Yano, D. Hong, S. Fukuzumi, *Phys. Chem. Chem. Phys.* **2012**, *14*, 5753–5760.
- [32] U. Maitra, B. Naidu, A. Govindaraj, C. Rao, *Proc. Mont. Acad. Sci.* **2013**, *110*, 11704–11707.
- [33] S. Zhuang, C. Huang, K. Huang, X. Hu, F. Tu, H. Huang, *Electrochem. Commun.* **2011**, *13*, 321–324.
- [34] W. Yang, J. Salim, S. Li, C. Sun, L. Chen, J. B. Goodenough, Y. Kim, *J. Mater. Chem.* **2012**, *22*, 18902–18907.
- [35] H. W. Park, D. U. Lee, M. G. Park, R. Ahmed, M. H. Seo, L. F. Nazar, Z. Chen, *ChemSusChem* **2015**, *8*, 1058–1065.
- [36] C. Kim, O. Gwon, I.-Y. Jeon, Y. Kim, J. Shin, Y.-W. Ju, J.-B. Baek, G. Kim, *J. Mater. Chem. A* **2016**, *4*, 2122–2127.
- [37] K. Gong, F. Du, Z. Xia, M. Durstock, L. Dai, *Science* **2009**, *323*, 760–764.
- [38] M. Y. Oh, S. K. Park, H. Park, H. Kim, K. Kang, J. H. Kim, K. C. Roh, T. H. Shin, *ACS Appl. Energy Mater.* **2018**, *1*, 5518–5526.
- [39] D. Wittmaier, T. Danner, N. Wagner, K. A. Friedrich, *J. Appl. Electrochem.* **2014**, *44*, 73–85.
- [40] Y. Liang, Y. Li, H. Wang, J. Zhou, J. Wang, T. Regier, H. Dai, *Nat. Mater.* **2011**, *10*, 780.
- [41] Y. J. Sa, K. Kwon, J. Y. Cheon, F. Kleitz, S. H. Joo, *J. Mater. Chem. A* **2013**, *1*, 9992–10001.
- [42] D. Wittmaier, S. Aisenbrey, N. Wagner, K. A. Friedrich, *Electrochim. Acta* **2014**, *149*, 355–363.
- [43] F. Cheng, J. Shen, B. Peng, Y. Pan, Z. Tao, J. Chen, *Nat. Chem.* **2011**, *3*, 79.
- [44] P. W. Menezes, A. Indra, A. Bergmann, P. Chernev, C. Walter, H. Dau, P. Strasser, M. Diress, *J. Mater. Chem. A* **2016**, *4*, 10014–10022.
- [45] T. W. Kim, M. A. Woo, M. Regis, K.-S. Choi, *J. Phys. Chem. Lett.* **2014**, *5*, 2370–2374.
- [46] C. Wei, Z. Feng, G. G. Scherer, J. Barber, Y. Shao-Horn, Z. J. Xu, *Adv. Mater.* **2017**, *29*, 1606800.
- [47] J. Xiao, Q. Kuang, S. Yang, F. Xiao, S. Wang, L. Guo, *Sci. Rep.* **2013**, *3*, 2300.
- [48] C. Sun, F. Li, C. Ma, Y. Wang, Y. Ren, W. Yang, Z. Ma, J. Li, Y. Chen, Y. Kim, *J. Mater. Chem. A* **2014**, *2*, 7188–7196.
- [49] W. Yang, J. Salim, C. Ma, Z. Ma, C. Sun, J. Li, L. Chen, Y. Kim, *Electrochem. Commun.* **2013**, *28*, 13–16.
- [50] L. Wang, X. Zhao, Y. Lu, M. Xu, D. Zhang, R. S. Ruoff, K. J. Stevenson, J. B. Goodenough, *J. Electrochem. Soc.* **2011**, *158*, A1379–A1382.
- [51] S. A. Makhlof, Z. H. Bakr, K. I. Aly, M. Moustafa, *Superlattices Microstruct.* **2013**, *64*, 107–117.
- [52] J. Zhang, Z. Zhao, Z. Xia, L. Dai, *Nat. Nanotechnol.* **2015**, *10*, 444.
- [53] Y. Su, Y. Zhu, H. Jiang, J. Shen, X. Yang, W. Zou, J. Chen, C. Li, *Nanoscale* **2014**, *6*, 15080–15089.
- [54] D. Ji, S. Peng, D. Safanama, H. Yu, L. Li, G. Yang, X. Qin, M. Srinivasan, S. Adams, S. Ramakrishna, *Chem. Mater.* **2017**, *29*, 1665–1675.
- [55] L. Qian, Z. Lu, T. Xu, X. Wu, Y. Tian, Y. Li, Z. Huo, X. Sun, X. Duan, *Adv. Energy Mater.* **2015**, *5*, 1500245.
- [56] B. Chen, R. Li, G. Ma, X. Gou, Y. Zhu, Y. Xia, *Nanoscale* **2015**, *7*, 20674–20684.
- [57] Q. Liu, J. Jin, J. Zhang, *ACS Appl. Mater. Interfaces* **2013**, *5*, 5002–5008.
- [58] M. Shen, C. Ruan, Y. Chen, C. Jiang, K. Ai, L. Lu, *ACS Appl. Mater. Interfaces* **2015**, *7*, 1207–1218.
- [59] P. Ganeshan, M. Prabu, J. Sanetuntikul, S. Shanmugam, *ACS Catal.* **2015**, *5*, 3625–3637.
- [60] A. M. El-Sawy, I. M. Mosa, D. Su, C. J. Guild, S. Khalid, R. Joesten, J. F. Rusling, S. L. Suib, *Adv. Energy Mater.* **2016**, *6*, 1501966.
- [61] K. Qu, Y. Zheng, S. Dai, S. Z. Qiao, *Nano Energy* **2016**, *19*, 373–381.
- [62] J. Yang, H. Sun, H. Liang, H. Ji, L. Song, C. Gao, H. Xu, *Adv. Mater.* **2016**, *28*, 4606–4613.
- [63] H. B. Yang, J. Miao, S.-F. Hung, J. Chen, H. B. Tao, X. Wang, L. Zhang, R. Chen, J. Gao, H. M. Chen, *Sci. Adv.* **2016**, *2*, e1501122.
- [64] R. Li, Z. Wei, X. Gou, *ACS Catal.* **2015**, *5*, 4133–4142.
- [65] W.-J. Jiang, L. Gu, L. Li, Y. Zhang, X. Zhang, L.-J. Zhang, J.-Q. Wang, J.-S. Hu, Z. Wei, L.-J. Wan, *J. Am. Chem. Soc.* **2016**, *138*, 3570–3578.
- [66] D. Singh, J. Tian, K. Mamiani, J. King, J. T. Miller, U. S. Ozkan, *J. Catal.* **2014**, *317*, 30–43.

- [67] K. Strickland, E. Miner, Q. Jia, U. Tylus, N. Ramaswamy, W. Liang, M.-T. Sougrati, F. Jaouen, S. Mukerjee, *Nat. Commun.* **2015**, *6*, 7343.
- [68] M. Lefèvre, E. Proietti, F. Jaouen, J.-P. Dodelet, *Science* **2009**, *324*, 71–74.
- [69] X. Lu, W.-L. Yim, B. H. Suryanto, C. Zhao, *J. Am. Chem. Soc.* **2015**, *137*, 2901–2907.
- [70] S. Ma, Y. Wu, J. Wang, Y. Zhang, Y. Zhang, X. Yan, Y. Wei, P. Liu, J. Wang, K. Jiang, S. Fan, Y. Xu, Z. Peng, *Nano Lett.* **2015**, *15*, 8084–8090.
- [71] Y. S. Jeong, J.-B. Park, H.-G. Jung, J. Kim, X. Luo, J. Lu, L. Curtiss, K. Amine, Y.-K. Sun, B. Scrosati, Y. J. Lee, *Nano Lett.* **2015**, *15*, 4261–4268.
- [72] B. D. McCloskey, R. Scheffler, A. Speidel, D. S. Bethune, R. M. Shelby, A. C. Luntz, *J. Am. Chem. Soc.* **2011**, *133*, 18038–18041.
- [73] Y.-C. Lu, Z. Xu, H. A. Gasteiger, S. Chen, K. Hamad-Schifferli, Y. Shao-Horn, *J. Am. Chem. Soc.* **2010**, *132*, 12170–12171.
- [74] Y.-C. Lu, H. A. Gasteiger, Y. Shao-Horn, *J. Am. Chem. Soc.* **2011**, *133*, 19048–19051.
- [75] A. Débart, J. Bao, G. Armstrong, P. G. Bruce, *J. Power Sources* **2007**, *174*, 1177–1182.
- [76] A. Débart, A. J. Paterson, J. Bao, P. G. Bruce, *Angew. Chem. Int. Ed.* **2008**, *47*, 4521–4524; *Angew. Chem.* **2008**, *120*, 4597–4600.
- [77] Y. Cui, Z. Wen, Y. Liu, *Energy Environ. Sci.* **2011**, *4*, 4727–4734.
- [78] R. A. Wong, C. Yang, A. Dutta, M. O. M. Hong, M. L. Thomas, K. Yamanaka, T. Ohta, K. Waki, H. R. Byon, *ACS Energy Lett.* **2018**, *3*, 592–597.
- [79] D. Aurbach, B. D. McCloskey, L. F. Nazar, P. G. Bruce, *Nat. Energy* **2016**, *1*, 16128.
- [80] W.-B. Luo, S.-L. Chou, J.-Z. Wang, Y.-C. Zhai, H.-K. Liu, *Small* **2015**, *11*, 2817–2824.
- [81] H.-B. Huang, S.-H. Luo, C.-L. Liu, T.-F. Yi, Y.-C. Zhai, *ACS Appl. Mater. Interfaces* **2018**, *10*, 21281–21290.
- [82] K. Adpakpong, S. M. Oh, D. A. Agyeman, X. Jin, N. Jarulertwathana, I. Y. Kim, T. Sarakonsri, Y.-M. Kang, S.-J. Hwang, *Adv. Funct. Mater.* **2018**, *28*, 1707106.
- [83] K. R. Yoon, G. Y. Lee, J.-W. Jung, N.-H. Kim, S. O. Kim, I.-D. Kim, *Nano Lett.* **2016**, *16*, 2076–2083.
- [84] W.-B. Luo, X.-W. Gao, S.-L. Chou, J.-Z. Wang, H.-K. Liu, *Adv. Mater.* **2015**, *27*, 6862–6869.
- [85] Y.-F. Xu, Y. Chen, G.-L. Xu, X.-R. Zhang, Z. Chen, J.-T. Li, L. Huang, K. Amine, S.-G. Sun, *Nano Energy* **2016**, *28*, 63–70.
- [86] L. Liu, J. Wang, Y. Hou, J. Chen, H.-K. Liu, J. Wang, Y. Wu, *Small* **2016**, *12*, 602–611.
- [87] B. D. Adams, C. Radtke, R. Black, M. L. Trudeau, K. Zaghib, L. F. Nazar, *Energy Environ. Sci.* **2013**, *6*, 1772–1778.
- [88] N. B. Aetukuri, B. D. McCloskey, J. M. García, L. E. Krupp, V. Viswanathan, A. C. Luntz, *Nat. Chem.* **2014**, *7*, 50.
- [89] L. Johnson, C. Li, Z. Liu, Y. Chen, S. A. Freunberger, P. C. Ashok, B. B. Praveen, K. Dholakia, J.-M. Tarascon, P. G. Bruce, *Nat. Chem.* **2014**, *6*, 1091.
- [90] S. Ganapathy, B. D. Adams, G. Stenou, M. S. Anastasaki, K. Goubitz, X.-F. Miao, L. F. Nazar, M. Wagemaker, *J. Am. Chem. Soc.* **2014**, *136*, 16335–16344.
- [91] G. K. P. Dathar, W. A. Shelton, Y. Xu, *J. Phys. Chem. Lett.* **2012**, *3*, 891–895.
- [92] E. Yilmaz, C. Yogi, K. Yamanaka, T. Ohta, H. R. Byon, *Nano Lett.* **2013**, *13*, 4679–4684.
- [93] C. Yang, R. A. Wong, M. Hong, K. Yamanaka, T. Ohta, H. R. Byon, *Nano Lett.* **2016**, *16*, 2969–2974.
- [94] F. Tian, M. D. Radin, D. J. Siegel, *Chem. Mater.* **2014**, *26*, 2952–2959.
- [95] Y. Wang, Z. Liang, Q. Zou, G. Cong, Y.-C. Lu, *J. Phys. Chem. C* **2016**, *120*, 6459–6466.
- [96] M. D. Radin, C. W. Monroe, D. J. Siegel, *Chem. Mater.* **2015**, *27*, 839–847.
- [97] V. Timoshhevskii, Z. Feng, K. H. Bevan, J. Goodenough, K. Zaghib, *App. Phys. Lett.* **2013**, *103*, 073901.
- [98] S. A. Cho, Y. J. Jang, H.-D. Lim, J.-E. Lee, Y. H. Jang, T.-T. H. Nguyen, F. M. Mota, D. P. Fenning, K. Kang, Y. Shao-Horn, D. H. Kim, *Adv. Energy Mater.* **2017**, *7*, 1700391.
- [99] R. Black, J.-H. Lee, B. Adams, C. A. Mims, L. F. Nazar, *Angew. Chem.* **2013**, *125*, 410–414; *Angew. Chem. Int. Ed.* **2013**, *52*, 392–396.
- [100] Y. J. Lee, D. H. Kim, T.-G. Kang, Y. Ko, K. Kang, Y. J. Lee, *Chem. Mater.* **2017**, *29*, 10542–10550.
- [101] W.-H. Ryu, T.-H. Yoon, S. H. Song, S. Jeon, Y.-J. Park, I.-D. Kim, *Nano Lett.* **2013**, *13*, 4190–4197.
- [102] K. P. C. Yao, M. Risch, S. Y. Sayed, Y.-L. Lee, J. R. Harding, A. Grimaud, N. Pour, Z. Xu, J. Zhou, A. Mansour, F. Bardé, Y. Shao-Horn, *Energy Environ. Sci.* **2015**, *8*, 2417–2426.
- [103] F. S. Gittleson, W.-H. Ryu, A. D. Taylor, *ACS Appl. Mater. Interfaces* **2014**, *6*, 19017–19025.
- [104] W.-H. Ryu, F. S. Gittleson, M. Schwab, T. Goh, A. D. Taylor, *Nano Lett.* **2015**, *15*, 434–441.
- [105] J.-L. Shui, N. K. Karan, M. Balasubramanian, S.-Y. Li, D.-J. Liu, *J. Am. Chem. Soc.* **2012**, *134*, 16654–16661.
- [106] J. Wang, Y. Zhang, L. Guo, E. Wang, Z. Peng, *Angew. Chem. Int. Ed.* **2016**, *55*, 5201–5205; *Angew. Chem.* **2016**, *128*, 5287–5291.
- [107] P. Forzatti, L. Lietti, *Catal. Today* **1999**, *52*, 165–181.
- [108] L. L. Hegedus, R. W. McCabe, *Studies in Surface Science and Catalysis*, Vol. 6 (Eds.: B. Delmon, G. F. Froment), Elsevier, **1980**, pp. 471–505.
- [109] D. S. Thakur, M. G. Thomas, *Appl. Catal.* **1985**, *15*, 197–225.
- [110] R. H. Crabtree, *Chem. Rev.* **2015**, *115*, 127–150.
- [111] Y. Chen, S. A. Freunberger, Z. Peng, O. Fontaine, P. G. Bruce, *Nat. Chem.* **2013**, *5*, 489.
- [112] Y. Qiao, S. Ye, *J. Phys. Chem. C* **2016**, *120*, 8033–8047.
- [113] H. Yang, Q. Wang, R. Zhang, B. D. Trimm, M. S. Whittingham, *Chem. Commun.* **2016**, *52*, 7580–7583.
- [114] Y. Qiao, Y. He, S. Wu, K. Jiang, X. Li, S. Guo, P. He, H. Zhou, *ACS Energy Lett.* **2018**, *3*, 463–468.
- [115] B. J. Bergner, A. Schürmann, K. Peppler, A. Garsuch, J. Janek, *J. Am. Chem. Soc.* **2014**, *136*, 15054–15064.
- [116] B. J. Bergner, C. Hofmann, A. Schürmann, D. Schröder, K. Peppler, P. R. Schreiner, J. Janek, *Phys. Chem. Chem. Phys.* **2015**, *17*, 31769–31779.
- [117] Y. Hase, J. Seki, T. Shiga, F. Mizuno, H. Nishikoori, H. Iba, K. Takechi, *Chem. Commun.* **2016**, *52*, 12151–12154.
- [118] B. J. Bergner, M. R. Busche, R. Pinedo, B. B. Berkes, D. Schröder, J. Janek, *ACS Appl. Mater. Interfaces* **2016**, *8*, 7756–7765.
- [119] C. Xu, G. Xu, Y. Zhang, S. Fang, P. Nie, L. Wu, X. Zhang, *ACS Energy Lett.* **2017**, *2*, 2659–2666.
- [120] Y. Chen, X. Gao, L. R. Johnson, P. G. Bruce, *Nat. Commun.* **2018**, *9*, 767.
- [121] D. J. Lee, H. Lee, Y.-J. Kim, J.-K. Park, H.-T. Kim, *Adv. Mater.* **2016**, *28*, 857–863.
- [122] H.-D. Lim, B. Lee, Y. Zheng, J. Hong, J. Kim, H. Gwon, Y. Ko, M. Lee, K. Cho, K. Kang, *Nat. Energy* **2016**, *1*, 16066.
- [123] S. H. Lee, J.-B. Park, H.-S. Lim, Y.-K. Sun, *Adv. Energy Mater.* **2017**, *7*, 1602417.
- [124] W.-J. Kwak, H.-G. Jung, D. Aurbach, Y.-K. Sun, *Adv. Energy Mater.* **2017**, *7*, 1701232.
- [125] X. Gao, Y. Chen, L. Johnson, Peter G. Bruce, *Nat. Mater.* **2016**, *15*, 882.
- [126] T. Liu, J. T. Frith, G. Kim, R. N. Kerber, N. Dubouis, Y. Shao, Z. Liu, P. C. M. M. Magusin, M. T. L. Casford, N. Garcia-Araez, C. P. Grey, *J. Am. Chem. Soc.* **2018**, *140*, 1428–1437.
- [127] S. Matsuda, K. Hashimoto, S. Nakanishi, *J. Phys. Chem. C* **2014**, *118*, 18397–18400.
- [128] X. Gao, Y. Chen, L. R. Johnson, Z. P. Jovanov, P. G. Bruce, *Nat. Energy* **2017**, *2*, 17118.
- [129] Y. Zhang, L. Wang, X. Zhang, L. Guo, Y. Wang, Z. Peng, *Adv. Mater.* **2018**, *30*, 1705571.
- [130] Y. Ko, H. Park, J. Kim, H. D. Lim, B. Lee, G. Kwon, S. Lee, Y. Bae, S. K. Park, K. Kang, *Adv. Funct. Mater.* **2018**, 1805623.
- [131] H.-D. Lim, H. Song, J. Kim, H. Gwon, Y. Bae, K.-Y. Park, J. Hong, H. Kim, T. Kim, Y. H. Kim, X. Lepró, R. Ovalle-Robles, R. H. Baughman, K. Kang, *Angew. Chem. Int. Ed.* **2014**, *126*, 4007–4012; *Angew. Chem. Int. Ed.* **2014**, *53*, 3926–3931.
- [132] H.-D. Lim, H. Park, H. Kim, J. Kim, B. Lee, Y. Bae, H. Gwon, K. Kang, *Angew. Chem. Int. Ed.* **2015**, *54*, 9663–9667; *Angew. Chem.* **2015**, *127*, 9799–9803.
- [133] Y. Bae, Y. S. Yun, H.-D. Lim, H. Lee, Y.-J. Kim, J. Kim, H. Park, Y. Ko, S. Lee, H. J. Kwon, H. Kim, H.-T. Kim, D. Im, K. Kang, *Chem. Mater.* **2016**, *28*, 8160–8169.
- [134] Y. Bae, D.-H. Ko, S. Lee, H.-D. Lim, Y.-J. Kim, H.-S. Shim, H. Park, Y. Ko, S. K. Park, H. J. Kwon, H. Kim, H.-T. Kim, Y.-S. Min, D. Im, K. Kang, *Adv. Energy Mater.* **2018**, *8*, 1702661.
- [135] H.-D. Lim, Y. S. Yun, S. Y. Cho, K.-Y. Park, M. Y. Song, H.-J. Jin, K. Kang, *Carbon* **2017**, *114*, 311–316.
- [136] T. Liu, M. Leskes, W. Yu, A. J. Moore, L. Zhou, P. M. Bayley, G. Kim, C. P. Grey, *Science* **2015**, *350*, 530–533.
- [137] Y. G. Zhu, Q. Liu, Y. Rong, H. Chen, J. Yang, C. Jia, L.-J. Yu, A. Karton, Y. Ren, X. Xu, S. Adams, Q. Wang, *Nat. Commun.* **2017**, *8*, 14308.
- [138] T. Zhang, K. Liao, P. He, H. Zhou, *Energy Environ. Sci.* **2016**, *9*, 1024–1030.

- [139] C. M. Burke, R. Black, I. R. Kochetkov, V. Giordani, D. Addison, L. F. Nazar, B. D. McCloskey, *ACS Energy Lett.* **2016**, *1*, 747–756.
- [140] M. Tułodziecki, G. M. Leverick, C. V. Amanchukwu, Y. Katayama, D. G. Kwabi, F. Bardé, P. T. Hammond, Y. Shao-Horn, *Energy Environ. Sci.* **2017**, *10*, 1828–1842.
- [141] C. K. Lee, Y. J. Park, *ACS Appl. Mater. Interfaces* **2016**, *8*, 8561–8567.
- [142] W.-J. Kwak, D. Hirshberg, D. Sharon, H.-J. Shin, M. Afri, J.-B. Park, A. Garsuch, F. F. Chesneau, A. A. Frimer, D. Aurbach, Y.-K. Sun, *J. Mater. Chem. A* **2015**, *3*, 8855–8864.
- [143] Z. Liang, Y.-C. Lu, *J. Am. Chem. Soc.* **2016**, *138*, 7574–7583.
- [144] W.-J. Kwak, D. Hirshberg, D. Sharon, M. Afri, A. A. Frimer, H.-G. Jung, D. Aurbach, Y.-K. Sun, *Energy Environ. Sci.* **2016**, *9*, 2334–2345.
- [145] S. Matsuda, S. Mori, Y. Kubo, K. Uosaki, K. Hashimoto, S. Nakanishi, *Chem. Phys. Lett.* **2015**, *620*, 78–81.
- [146] D. Sun, Y. Shen, W. Zhang, L. Yu, Z. Yi, W. Yin, D. Wang, Y. Huang, J. Wang, D. Wang, J. B. Goodenough, *J. Am. Chem. Soc.* **2014**, *136*, 8941–8946.
- [147] W.-H. Ryu, F. S. Gittleson, J. M. Thomsen, J. Li, M. J. Schwab, G. W. Brudvig, A. D. Taylor, *Nat. Commun.* **2016**, *7*, 12925.
- [148] N. Feng, P. He, H. Zhou, *ChemSusChem* **2015**, *8*, 600–602.
- [149] W. Yu, W. Yang, R. Liu, L. Qin, Y. Lei, L. Liu, D. Zhai, B. Li, F. Kang, *Electrochem. Commun.* **2017**, *79*, 68–72.
- [150] Y. G. Zhu, C. Jia, J. Yang, F. Pan, Q. Huang, Q. Wang, *Chem. Commun.* **2015**, *51*, 9451–9454.
- [151] Y. G. Zhu, X. Wang, C. Jia, J. Yang, Q. Wang, *ACS Catal.* **2016**, *6*, 6191–6197.
- [152] S. H. Lee, W.-J. Kwak, Y.-K. Sun, *J. Mater. Chem. A* **2017**, *5*, 15512–15516.
- [153] J. Zhang, B. Sun, Y. Zhao, K. Kretschmer, G. Wang, *Angew. Chem. Int. Ed.* **2017**, *56*, 8505–8509; *Angew. Chem.* **2017**, *129*, 8625–8629.
- [154] Z. Liu, L. Ma, L. Guo, Z. Peng, *J. Phys. Chem. Lett.* **2018**, *9*, 5915–5920.

Manuscript received: November 24, 2018

Revised manuscript received: January 16, 2019

Accepted manuscript online: January 24, 2019

Version of record online: February 6, 2019